Supplementary Information

Porous carbon composites as clean energy materials with extraordinary methane storage capacity

Ibtisam Alali,[1,2] Amina U. Shehu[1] and Robert Mokaya[1]*

[1]School of Chemistry, University of Nottingham, University Park, Nottingham NG7 2RD, U. K.

[2]Chemistry Department, College of Science, Jouf University, P.O. BOX 2014, Sakaka, Saudi Arabia.

E-mail: r.mokaya@nottingham.ac.uk (R. Mokaya)

Supplementary Table 1. Surface area and pore volume of carbon composite PET4800 and after compaction (CPET4800) compared to similarly prepared (i.e. activation temperature of 800 ^{o}C (T) and KOH/carbon ratio (x) of 4) activated carbons derived from a range of precursors.

Sample	Precursor	Surface area[a] (m^2 g^{-1})	Pore volume[b] (cm^3 g^{-1})	Reference
PET4800	PET hydrochar	2828 (2352)	1.47 (1.07)	This work
CPET4800	PET hydrochar	2793 (2292)	1.47 (1.06)	This work
ACDS4800	Air –carbonised date seed	2609 (1825)	1.10 (0.70)	1,2
ACSD-4800	Air-carbonised sawdust	2610 (1892)	1.15 (0.74)	3
CNL1-4800	Burnt wood	2183 (1886)	1.05 (0.84)	4
SD4800D	Sawdust (Directly activated)	2980 (478)	2.10 (0.30)	5
SD4800	Sawdust hydrochar	2783 (694)	1.80 (0.36)	6
LAC4800	Lignin hydrochar	3235 (1978)	1.77 (0.93)	7
ACGR4800	Jujun grass hydrochar	2957 (1578)	1.72 (0.75)	8
C-4800	Cellulose hydrochar	2125 (1707)	0.98 (0.74)	3,9
CA-4800	Cellulose acetate hydrochar	2864 (2662)	1.32 (1.17)	9
SF-4800	Smoked cigarette butt hydrochar	2393 (1810)	1.09 (0.70)	10

The values in the parenthesis refer to: [a]micropore surface area and [b]micropore volume.

Supplementary Table 2. Surface area and pore volume of carbon composite PET4700 and after compaction (CPET4700) compared to similarly prepared (i.e. activation temperature of 700 ^{o}C (T) and KOH/carbon ratio (x) of 4) activated carbons derived from a range of precursors.

Sample	Precursor	Surface area[a] (m^2 g^{-1})	Pore volume[b] (cm^3 g^{-1})	Reference
PET4700	PET hydrochar	2650 (2129)	1.43 (0.96)	This work
CPET4700	PET hydrochar	2590 (2079)	1.38 (0.93)	This work
ACDS4700	Air-carbonised date seed	2192 (1871)	0.93 (0.74)	1,2
SD4700	Sawdust hydrochar	2252 (2088)	1.03 (0.91)	6
LAC4700	Lignin hydrochar	2038 (1832)	1.00 (0.84)	7
ACGR4700	Jujun grass hydrochar	3144 (2753)	1.56 (1.23)	3
C-4700	Cellulose hydrochar	2370 (2201)	1.08 (0.94)	3,9
CA-4700	Cellulose acetate hydrochar	3771 (3484)	1.75 (1.54)	9
S4700	Starch hydrochar	2194 (2082)	1.01 (0.92)	6
FF-4700	Fresh cigarette filter hydrochar	2803 (1901)	1.23 (0.73)	10
SF-4700	Smoked cigarette butt hydrochar	2512 (2019)	1.20 (0.91)	10

The values in the parenthesis refer to: [a]micropore surface area and [b]micropore volume.

Supplementary Table 3. Textural properties of PET-derived activated carbon composites prepared at KOH/hydrochar (HC) ratio of 2 and 4 and activation temperature of 600, 700 or 800 ^{o}C. Samples prepared at KOH/HC ratio of 2 had relatively low porosity (surface area and pore volume) and were therefore not explored further for methane storage.

Sample	KOH/HC ratio	Surface area (m^2 g^{-1})	Micropore surface area[a] (m^2 g^{-1})	Pore volume (cm^3 g^{-1})	Micropore volume[b] (cm^3 g^{-1})
PET2600	2	819	794 (97)	0.35	0.31 (89)
PET2700	2	1038	985 (95)	0.51	0.38 (75)
PET2800	2	1482	1359 (92)	0.75	0.54 (72)
PET4600	4	2154	1758 (82)	1.11	0.78 (70)
CPET4600	4	2045	1618 (79)	1.11	0.73 (66)
PET4700	4	2650	2129 (80)	1.43	0.96 (67)
CPET4700	4	2590	2079 (80)	1.38	0.93 (67)
PET4800	4	2828	2352 (83)	1.47	1.07 (73)
CPET4800	4	2793	2292 (82)	1.47	1.06 (72)

The values in the parenthesis refer to: [a] % micropore surface area, and [b] % micropore volume.

Supplementary Table 4. Expected packing density for powder forms of the PET*4T* activated carbon composites estimated from their respective carbon and alumina content, and the density of alumina (3.95 g cm^{-3}).

Sample	Alumina content [a] (wt%)	Packing density if PET*4T* are fully carbonaceous[b] (g cm^{-3})	Estimated packing density of composite (g cm^{-3})	Experimentally determined packing density of compacted composite (g cm^{-3})[c]
PET4600	9.5	0.63	0.95	1.13
PET4700	8.0	0.52	0.79	1.01
PET4800	7.5	0.51	0.78	0.98

[a] The particle density of alumina is 3.95 g cm^{-3}. [b] The packing density assuming the samples were fully carbonaceous was estimated using the equation; $d_{carbon} = (1/\rho s + V_T)^{-1}$, where d_{carbon} is packing density, ρs is skeletal density (2.1 g cm^{-3}) and V_T is total pore volume. Packing density of the compacted (at 370 MPa for 10 min) composites (in the form of well-formed pellets/discs) was obtained from their mass and volume (volume = $\pi r^2 h$, where r is radius of the disc, i.e., 0.65 cm, and h is the height of the disc).

Supplementary Table 5. Yield and elemental composition of sawdust hydrochar (SDH)-derived activated carbon (SDHAC) and activated carbon composites (SDHACCx).

Sample	Yield [wt %]	C [%]	H [%]	O [%][a]	O/C ratio[b]
SDHAC	21	92.2	0	7.8	0.06
SDHACC20	31	86.5	0	13.5	0.12
SDHACC15	25	89.0	0	11.0	0.09
SDHACC8	24	82.6	0	17.4	0.16

[a] Obtained as difference (i.e., 100-C-H-M). [b]Atomic ratio.

Supplementary Table 6. Textural properties of sawdust hydrochar derived activated carbon (SDHAC) and activated carbon composites (SDHACCx).

Sample	Surface area (m^2 g^{-1})	Micropore surface area[a] (m^2 g^{-1})	Pore volume (cm^3 g^{-1})	Micropore volume[b] (cm^3 g^{-1})	Surface area density[c] (m^2 cm^{-3})
SDHAC	2898	885 (31)	1.40	0.33 (24)	2070
SDHACC20	2655	1053 (40)	1.23	0.40 (33)	2159
SDHACC15	2602	1198 (46)	1.21	0.47 (39)	2150
SDHACC8	2230	1679 (75)	1.00	0.69 (69)	2230

The values in the parenthesis refer to: [a] % micropore surface area, and [b] % micropore volume. [c] Surface area density is obtained as ratio of total surface area to total pore volume.

Supplementary Table 7. Total gravimetric methane uptake of compacted PET-derived activated carbon composites at 25 ^{o}C and various uptake pressures.

Sample	Total gravimetric methane uptake ($g\ g^{-1}$)			
	35 bar	65 bar	80 bar	100 bar
CPET4600	0.16	0.22	0.24	0.26
CPET4700	0.19	0.26	0.28	0.31
CPET4800	0.21	0.27	0.30	0.33

Supplementary Table 8. Methane uptake of PET-derived activated carbon composites compared to selected benchmark MOFs and carbons reported in the literature. Volumetric uptake of powder MOFs is calculated based on crystallographic density.

Sample	Density ($g\ cm^{-3}$)	65 bar		80 bar		100 bar		Reference
		($g\ g^{-1}$)	($cm^3\ cm^{-3}$)	($g\ g^{-1}$)	($cm^3\ cm^{-3}$)	($g\ g^{-1}$)	($cm^3\ cm^{-3}$)	
CPET4600	1.13	0.22	344	0.24	378	0.26	412	This work
CPET4700	1.01	0.26	362	0.28	399	0.31	442	This work
CPET4800	0.98	0.28	374	0.30	408	0.33	447	This work
CNL4800	0.67	0.26	241	0.29	269	0.31	291	2
PPYCNL124	0.52	0.30	217	0.33	238	0.36	260	2
PPYCNL214	0.36	0.36	183	0.41	204	0.46	229	2
ACDS4800	0.69	0.25	243	0.27	262	0.29	282	1,2
PPYSD114	0.47	0.32	211	0.35	231	0.39	254	2
AX-21 carbon	0.487	0.30	203	0.33	222	0.35	238	12
HKUST-1	0.881	0.21	263	0.22	272	0.23	281	12
Ni-MOF-74	1.195	0.15	259	0.16	267	0.17	277	12
Al-soc-MOF-1	0.34	0.41	197	0.47	222			13
MOF-210	0.25	0.41	143	0.48	168			14
NU-1500-Al	0.498	0.29	200	0.31	216	0.34	237	15
NU-1501-Fe	0.299	0.40	168	0.46	193	0.52	218	15
NU-1501-Al	0.283	0.41	163	0.48	190	0.54	214	15
$_{mono}$HKUST-1	1.06	0.17	261	0.18	278	0.18	275	16
$_{mono}$UiO-66_D	1.05	0.14	210	0.17	245	0.20	296	17

Supplementary Table 9. Methane uptake working capacity of PET-derived activated carbon composites compared to selected benchmark MOFs and carbons reported in the literature. Volumetric uptake of powder MOFs is calculated based on crystallographic density.

Sample	65 bar		80 bar		100 bar		Reference
	($g\ g^{-1}$)	($cm^3\ cm^{-3}$)	($g\ g^{-1}$)	($cm^3\ cm^{-3}$)	($g\ g^{-1}$)	($cm^3\ cm^{-3}$)	
CPET4600	0.17	264	0.19	298	0.21	332	This work
CPET4700	0.20	278	0.22	315	0.25	358	This work
CPET4800	0.18	280	0.23	314	0.26	353	This work
CNL4800	0.19	182	0.22	202	0.24	224	2
PPYCNL124	0.23	167	0.26	188	0.29	209	2
PPYCNL214	0.29	146	0.34	167	0.39	192	2
ACDS4800	0.18	171	0.20	189	0.22	209	1,2
PPYSD114	0.25	162	0.28	182	0.32	205	2
AX-21 carbon	0.23	155	0.26	174	0.28	190	12
HKUST-1	0.15	189	0.16	198	0.17	207	12
Ni-MOF-74	0.08	144	0.09	152	0.10	162	12
Al-soc-MOF-1	0.36	176	0.42	201			13
MOF-210	0.38	134	0.45	157			14
NU-1500-Al	0.24	165	0.26	181	0.29	202	15
NU-1501-Fe	0.36	151	0.42	176	0.48	201	15
NU-1501-Al	0.37	147	0.44	174	0.50	198	15
$_{mono}$HKUST-1	0.12	184	0.13	201	0.13	198	16
$_{mono}$UiO-66_D	0.11	167	0.14	202	0.17	253	17

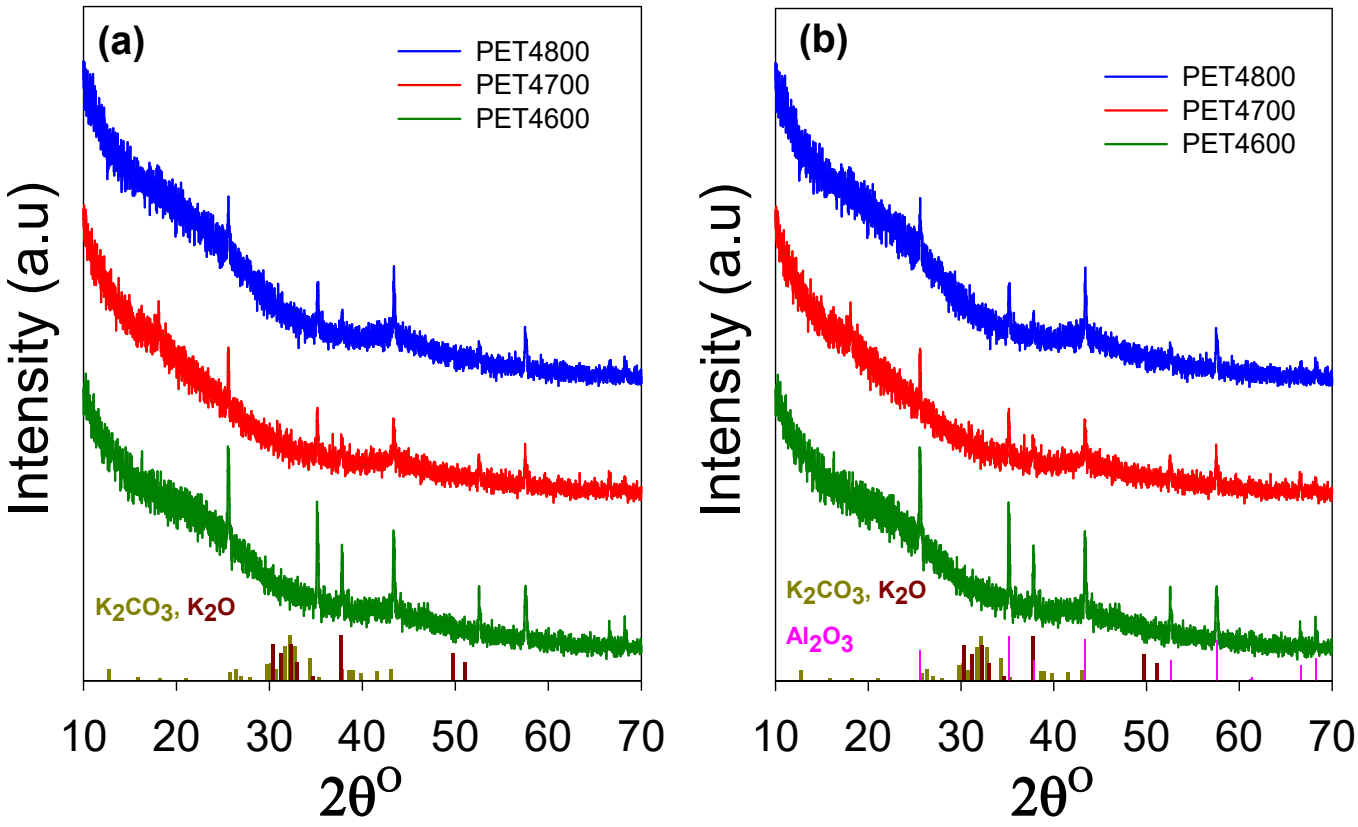

Supplementary Fig. 1 Nature of PET-derived activated carbon composites. Powder XRD pattern of PET-derived carbon composites indexed to (a) K_2CO_3 and K_2O, and (b) K_2CO_3, K_2O and Al_2O_3. The indexing supports the presence of Al_2O_3, although the K salts may also be present but to a much lower extent.

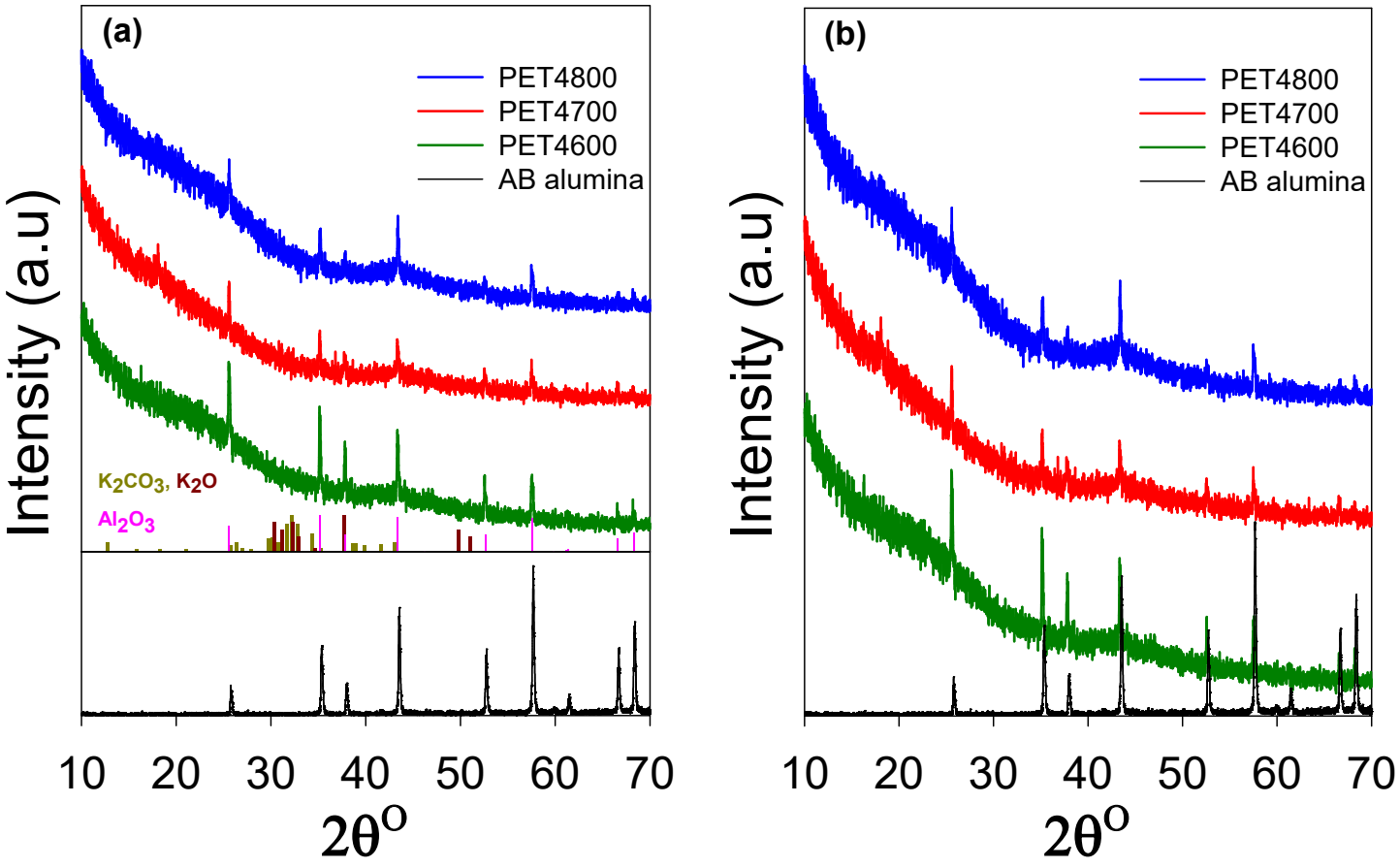

Supplementary Fig. 2 Confirmation of presence of alumina from a ground alumina boat (designated as AB alumina) in PET-derived activated carbon composites. (a) Powder XRD pattern of AB alumina compared to those of the PET-derived carbon composites, and index peaks of K_2CO_3, K_2O and Al_2O_3; (b) Powder XRD patterns of AB alumina and PET-derived activated carbon composites.

The XRD patterns confirm that the sharp peaks are due to the presence of alumina that comes from the alumina boat.

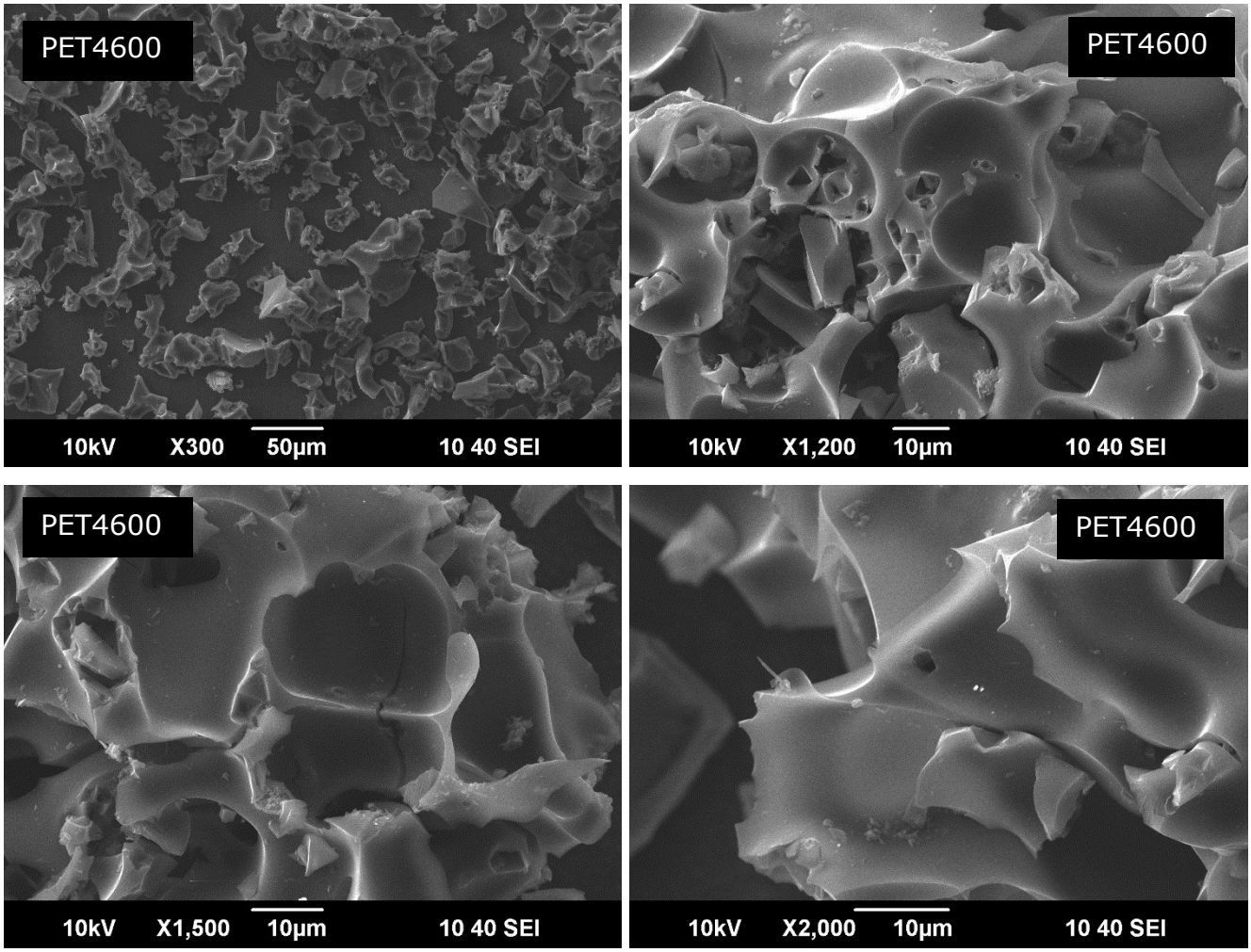

Supplementary Fig. 3 SEM images of activated carbon composite PET4600. The activated carbon composite was prepared from activation of PET-derived hydrochar at 600 ^{o}C and KOH/hydrochar ratio of 4.

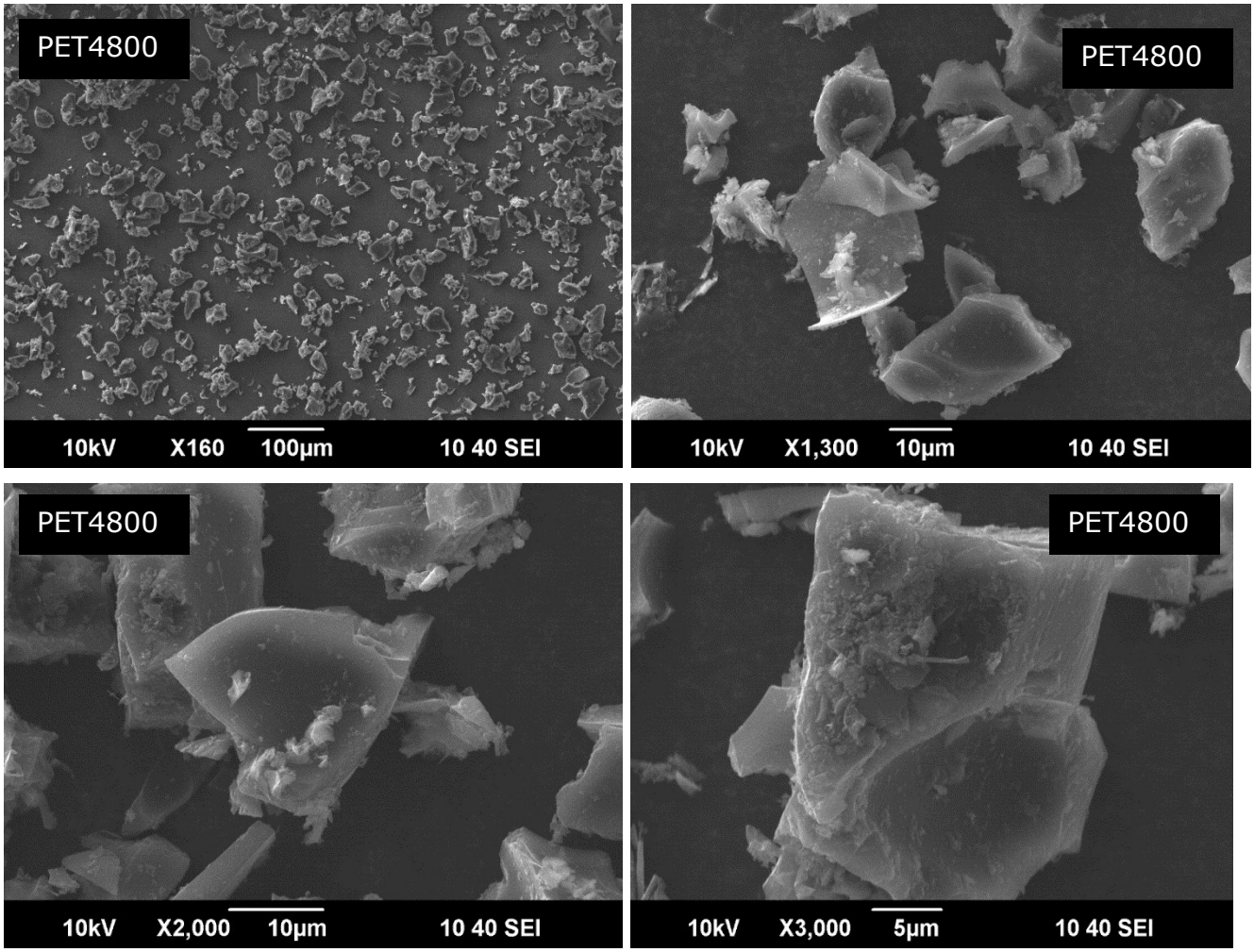

Supplementary Fig. 4 SEM images of activated carbon composite PET4800. The activated carbon composite was prepared from activation of PET-derived hydrochar at 800 ^{o}C and KOH/hydrochar ratio of 4.

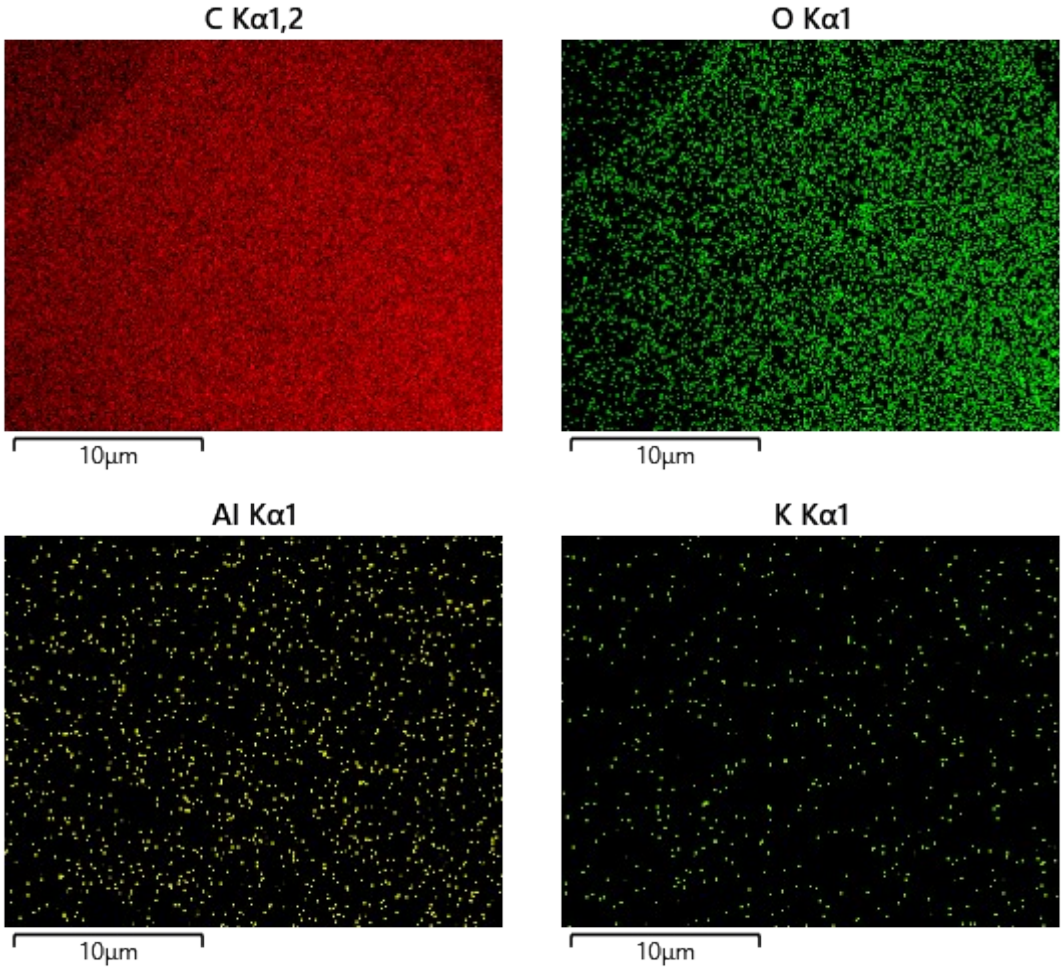

Supplementary Fig. 5 Elemental mapping of activated carbon composite PET4600. The activated carbon composite was prepared from activation of PET-derived hydrochar at 600 °C and KOH/hydrochar ratio of 4.

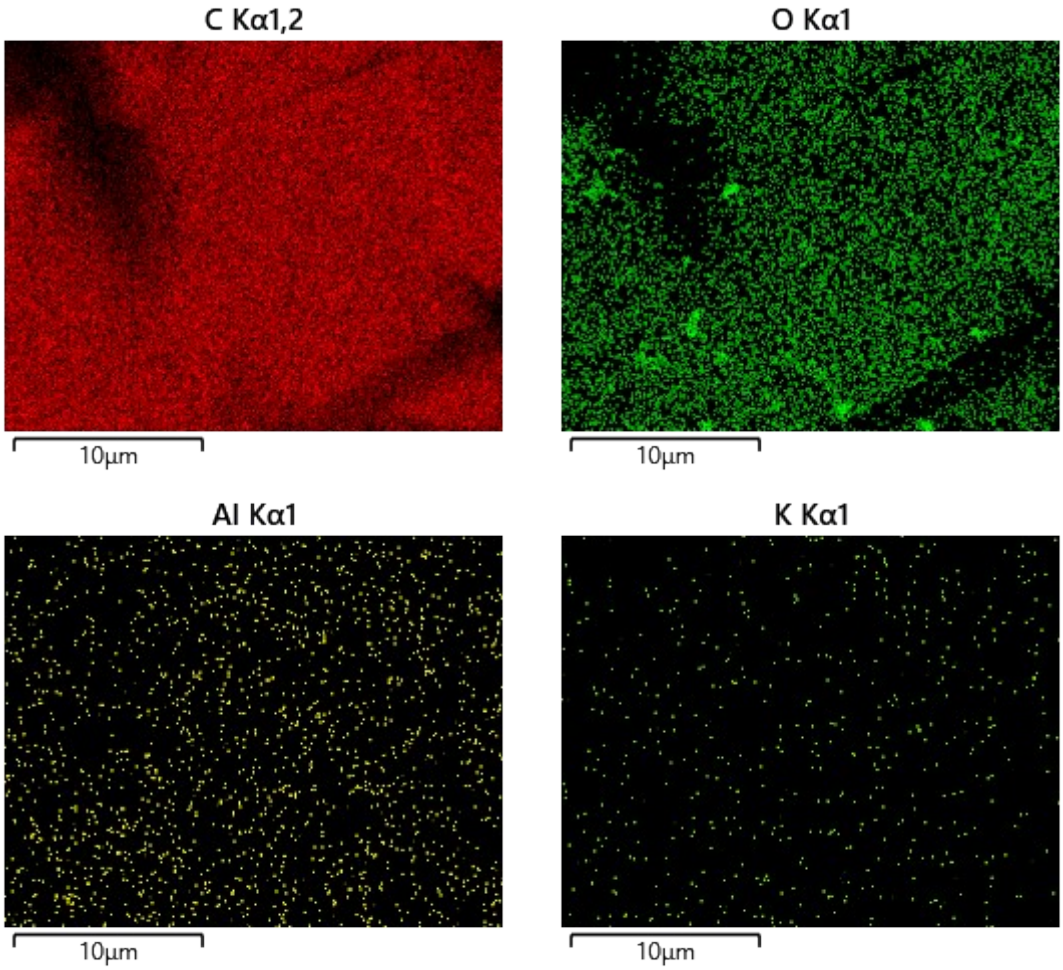

Supplementary Fig. 6 Elemental mapping of activated carbon composite PET4700. The activated carbon composite was prepared from activation of PET-derived hydrochar at 700 °C and KOH/hydrochar ratio of 4.

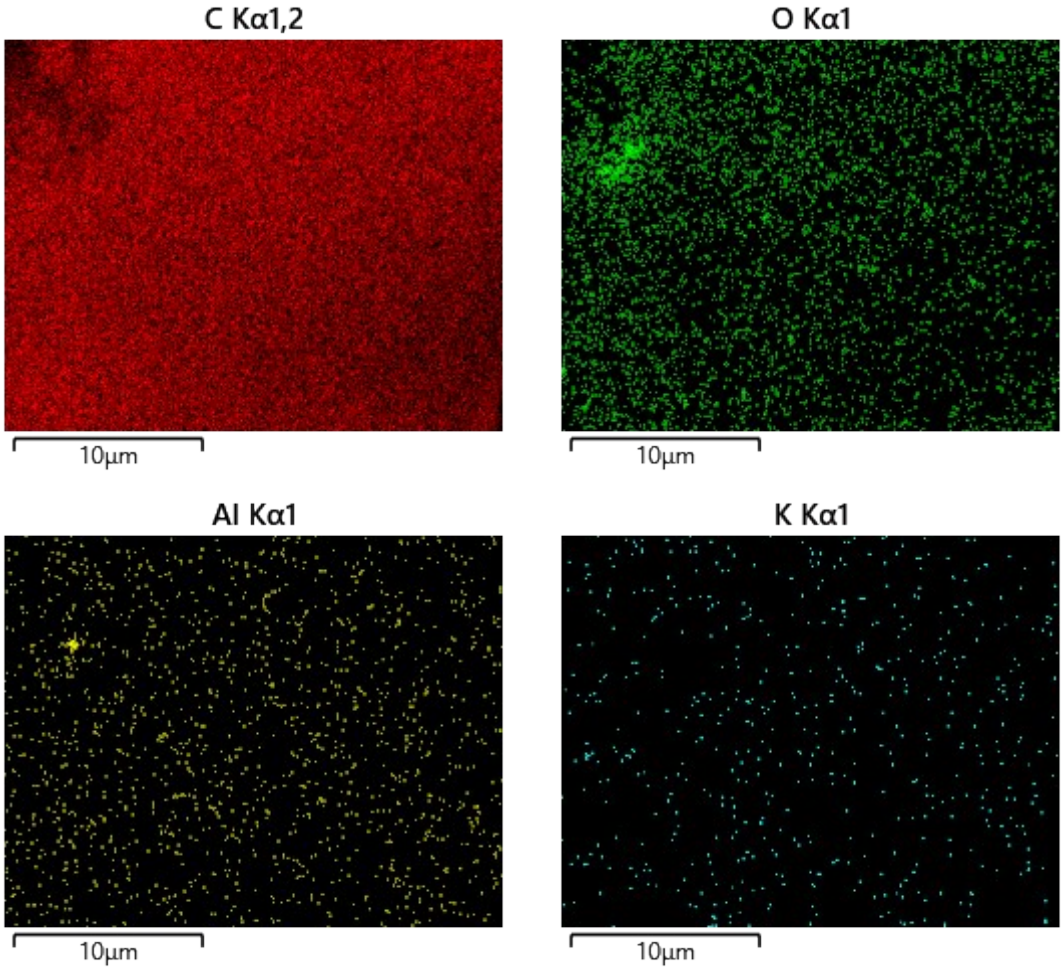

Supplementary Fig. 7 Elemental mapping of activated carbon composite PET4800. The activated carbon composite was prepared from activation of PET-derived hydrochar at 800 °C and KOH/hydrochar ratio of 4.

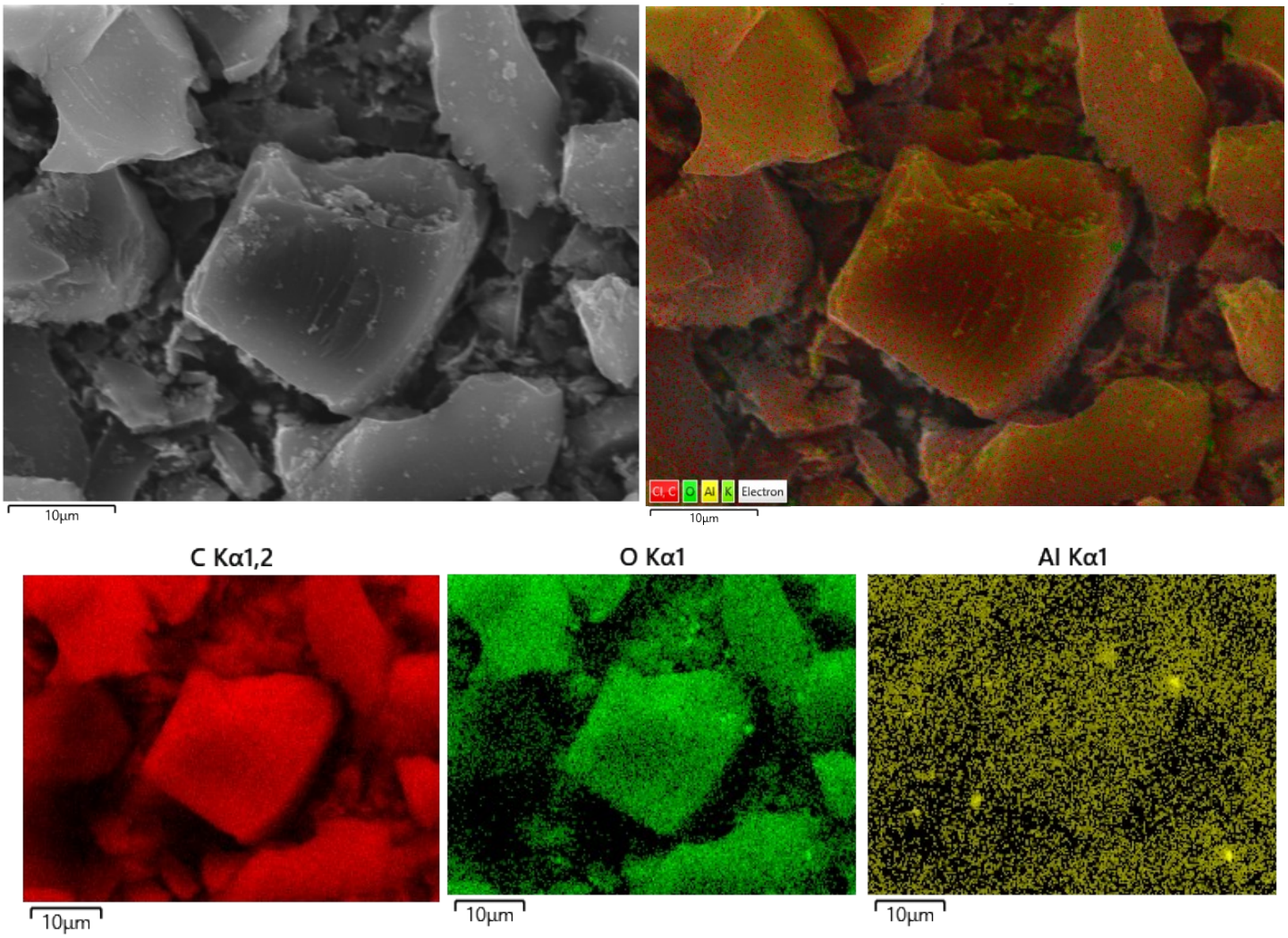

Supplementary Fig. 8 SEM image and elemental mapping of PET4700 activated carbon composite. The images suggest a homogeneous distribution of the carbon and alumina components, and the apparent absence of large particles of alumina.

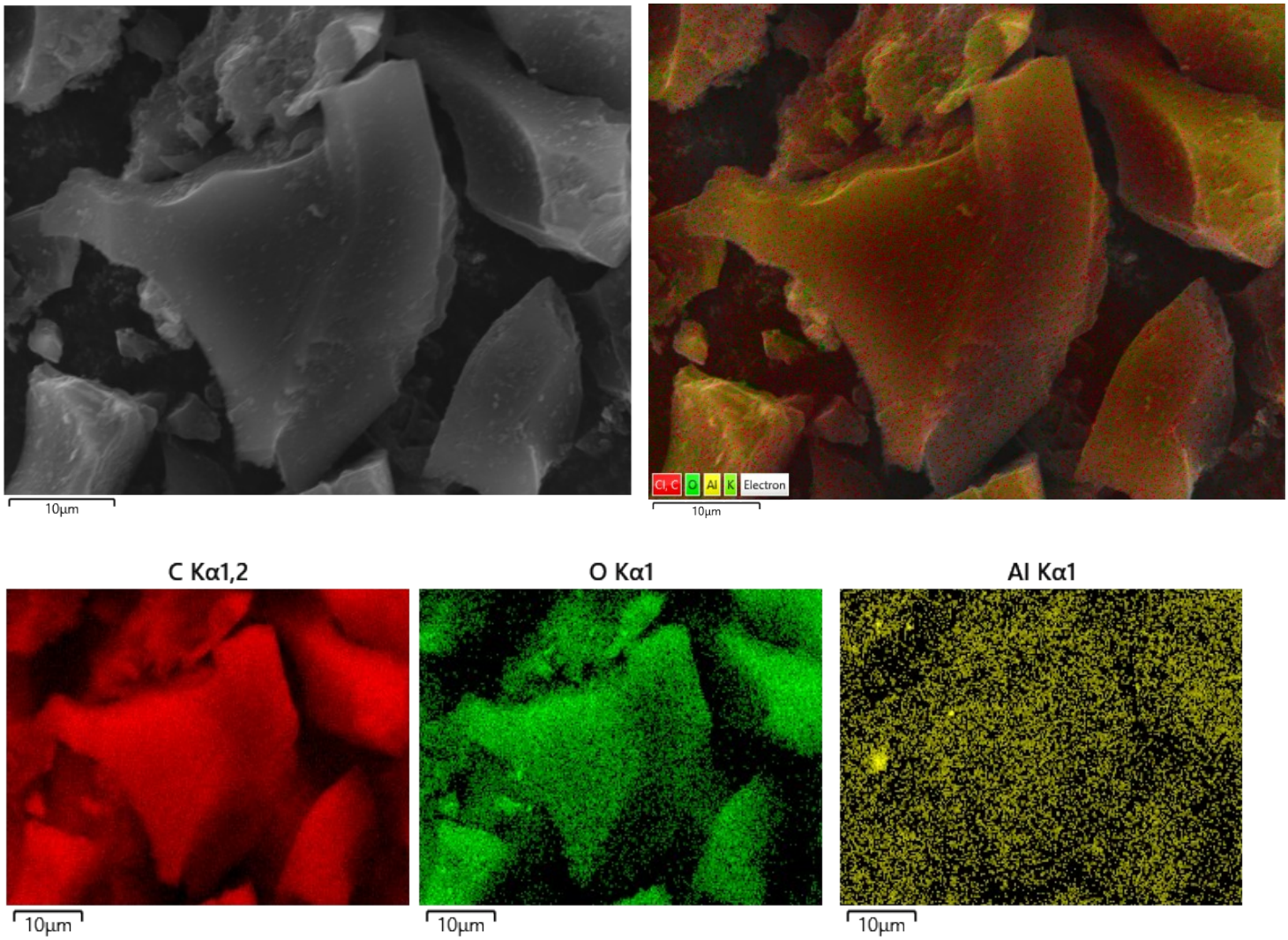

Supplementary Fig. 9 SEM image and elemental mapping of PET4800 activated carbon composite. The images indicate a homogeneous distribution of the carbon and alumina components, and the apparent absence of large particles of alumina.

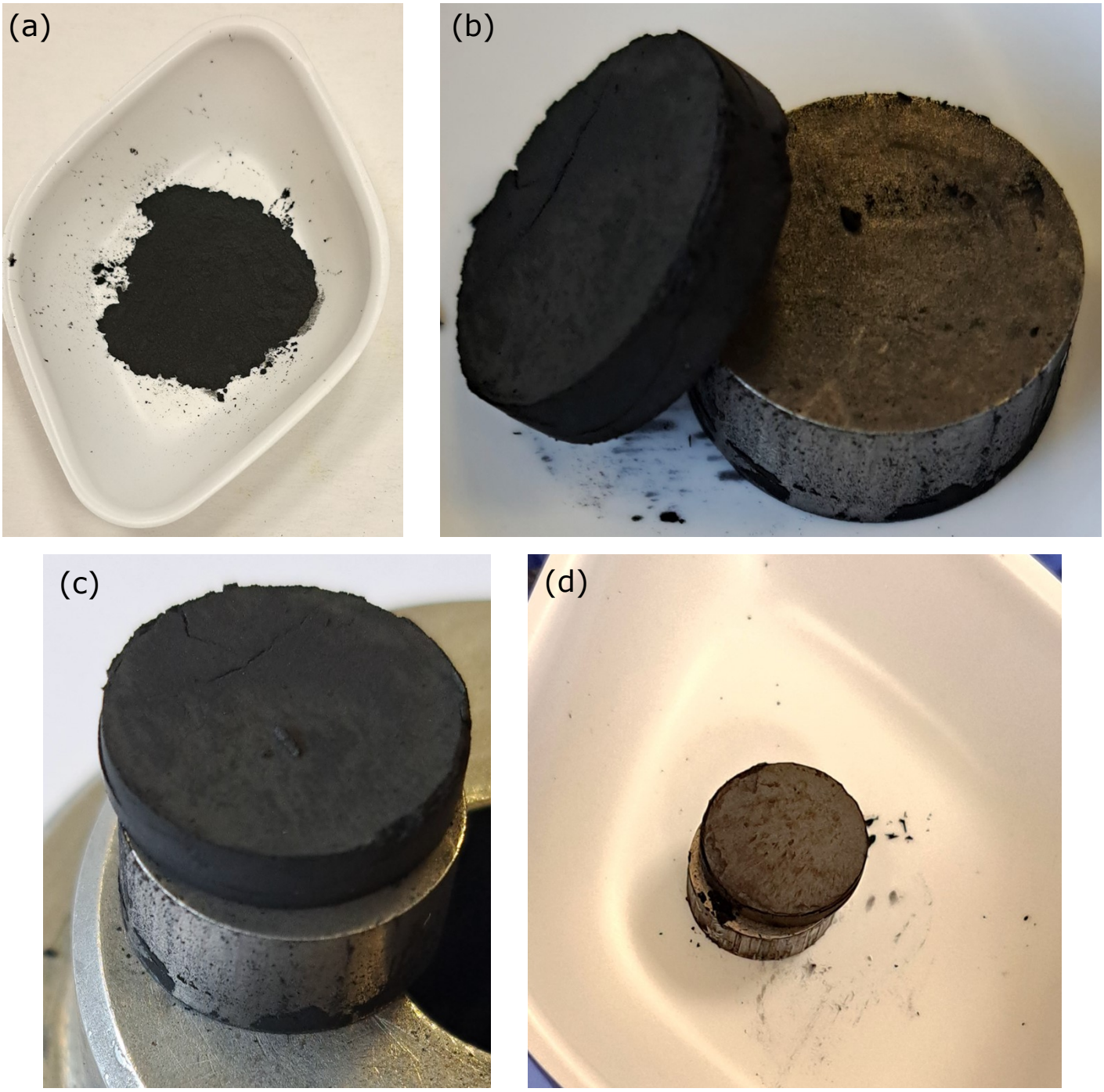

Supplementary Fig. 10 Representative photos of an activated carbon composite before (a) and after (b, c and d) compaction at 370 MPa for 10 min.

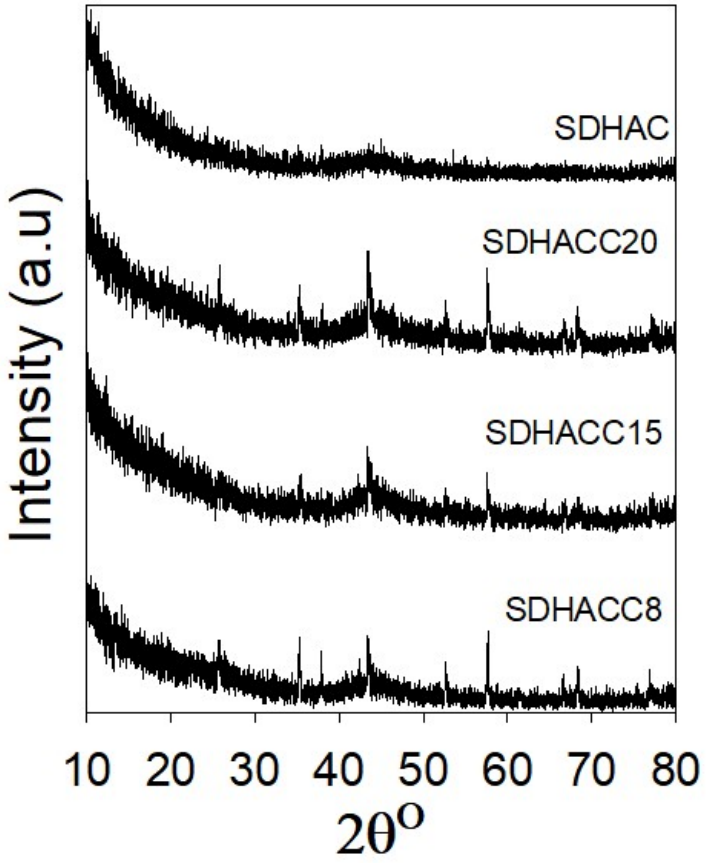

Supplementary Fig. 11 Powder XRD pattern of sawdust hydrochar (SDH)-derived carbon products prepared at KOH/SDH ratio of 4 and 800 °C with added alumina (SDHACCx) or no alumina (SDHAC). The patterns of SDHACCx series samples have sharp peaks indicating the presence of alumina but which are absent for SDHAC.

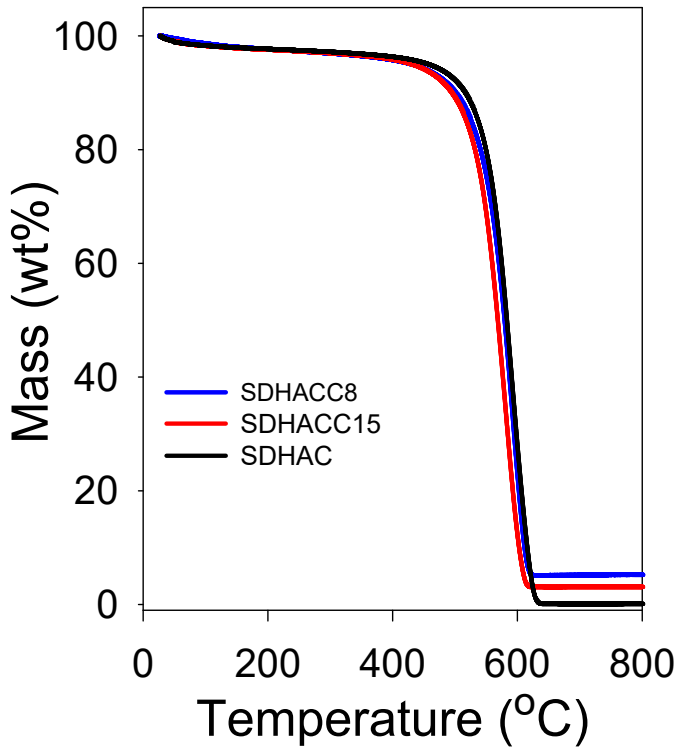

Supplementary Fig. 12 TGA curves of sawdust hydrochar (SDH)-derived carbon products prepared at KOH/SDH ratio of 4 and 800 °C with added alumina (SDHACCx) or no alumina (SDHAC). The curves of SDHACCx series samples show the retention of residual mass (ascribed to alumina) at 800 °C, while SDHAC, being fully carbonaceous is completely burnt off.

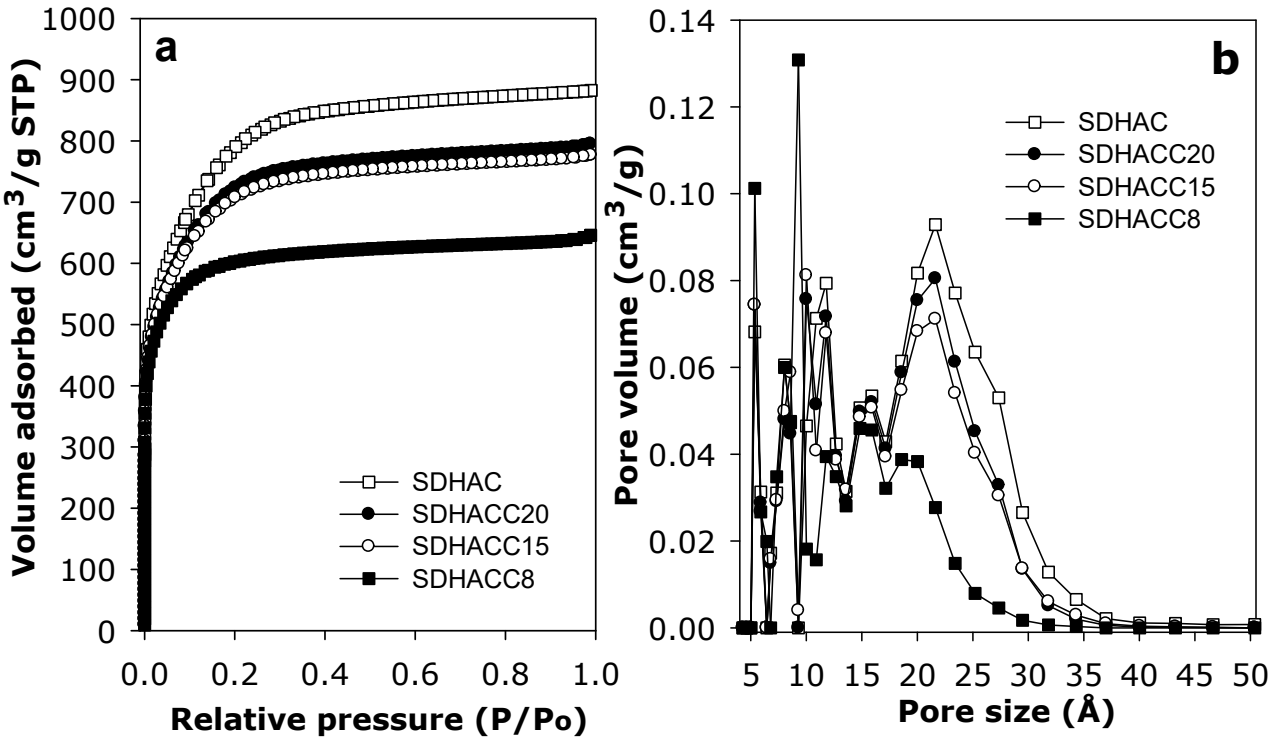

Supplementary Fig. 13 Nitrogen sorption isotherms (a) and pore size distribution curves (b) of sawdust hydrochar (SDH)-derived carbon products prepared at KOH/SDH ratio of 4 and 800 ^{o}C with added alumina (SDHACCx) or no alumina (SDHAC).

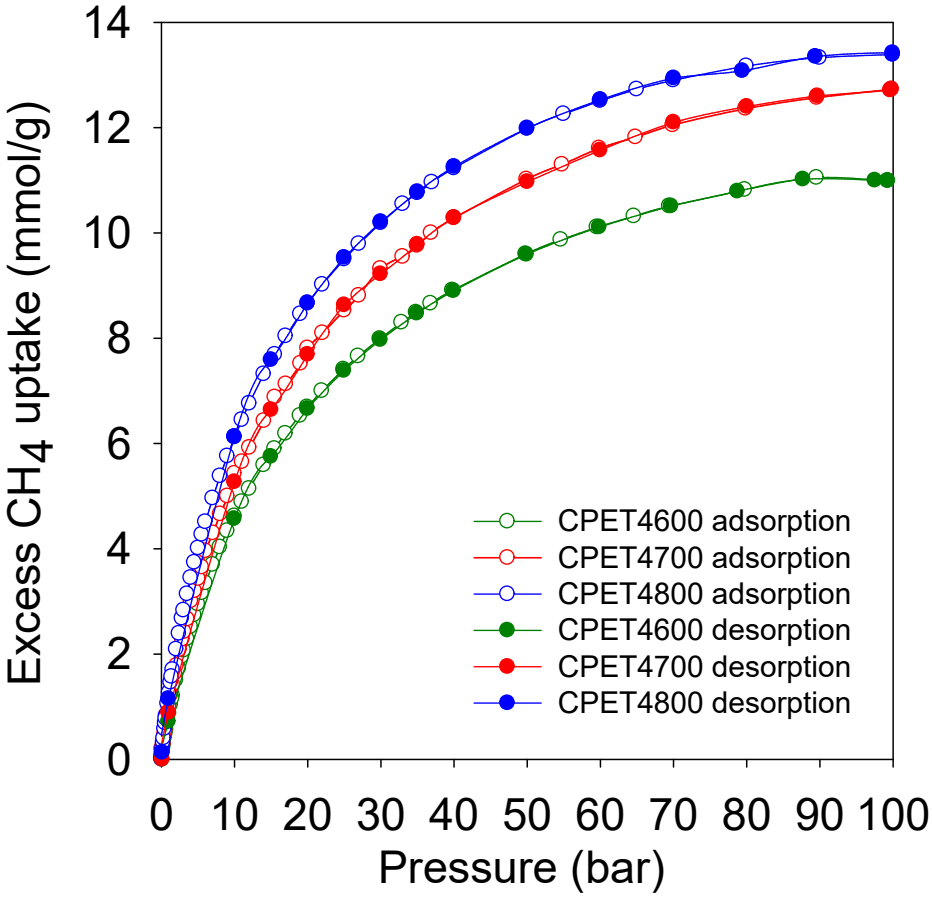

Supplementary Fig. 14 Methane uptake of PET-derived carbon composites. Gravimetric methane uptake isotherms showing both adsorption and desorption branches

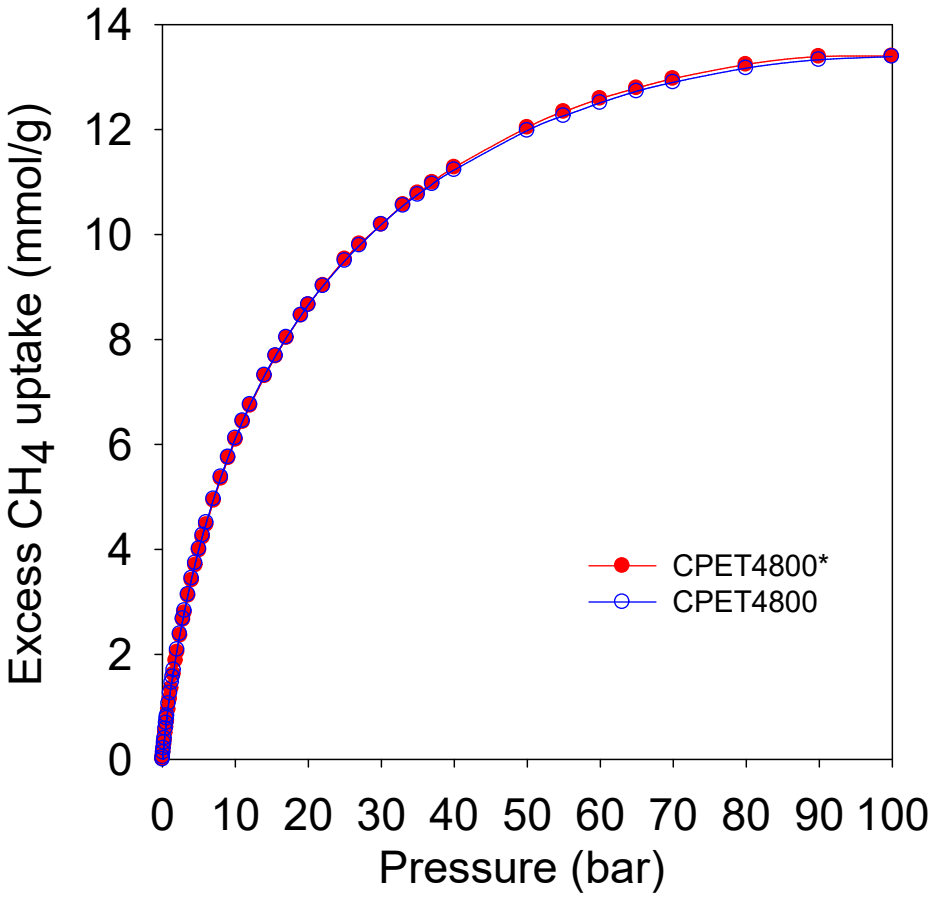

Supplementary Fig. 15 Methane uptake of sample CPET4800. Gravimetric methane uptake isotherms showing the repeatability of the uptake measurements; (* means repeat analysis). The isotherms are reproducible to a high degree.

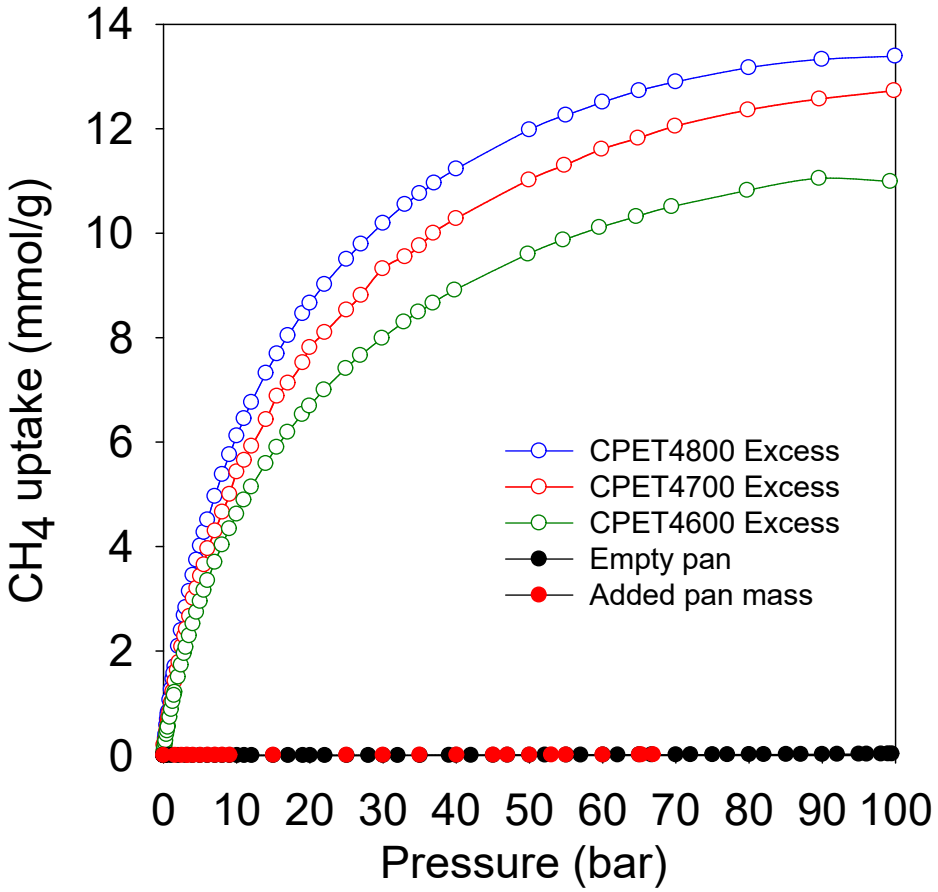

Supplementary Fig. 16 Methane uptake measurements with no samples added to sample holder. Excess gravimetric methane uptake isotherms with empty sample holders. The measurements were performed in two ways – one with an empty sample holder and another where a weight of the same material as the sample holder was added to the sample holder. In both cases, there was hardly any excess methane uptake, only recording 0.03 mmol at 100 bar, which is equivalent to 0.27% of the excess uptake of CPET4600, 0.24% of the uptake of CPET4700 and 0.22% of the uptake of CPET4800.

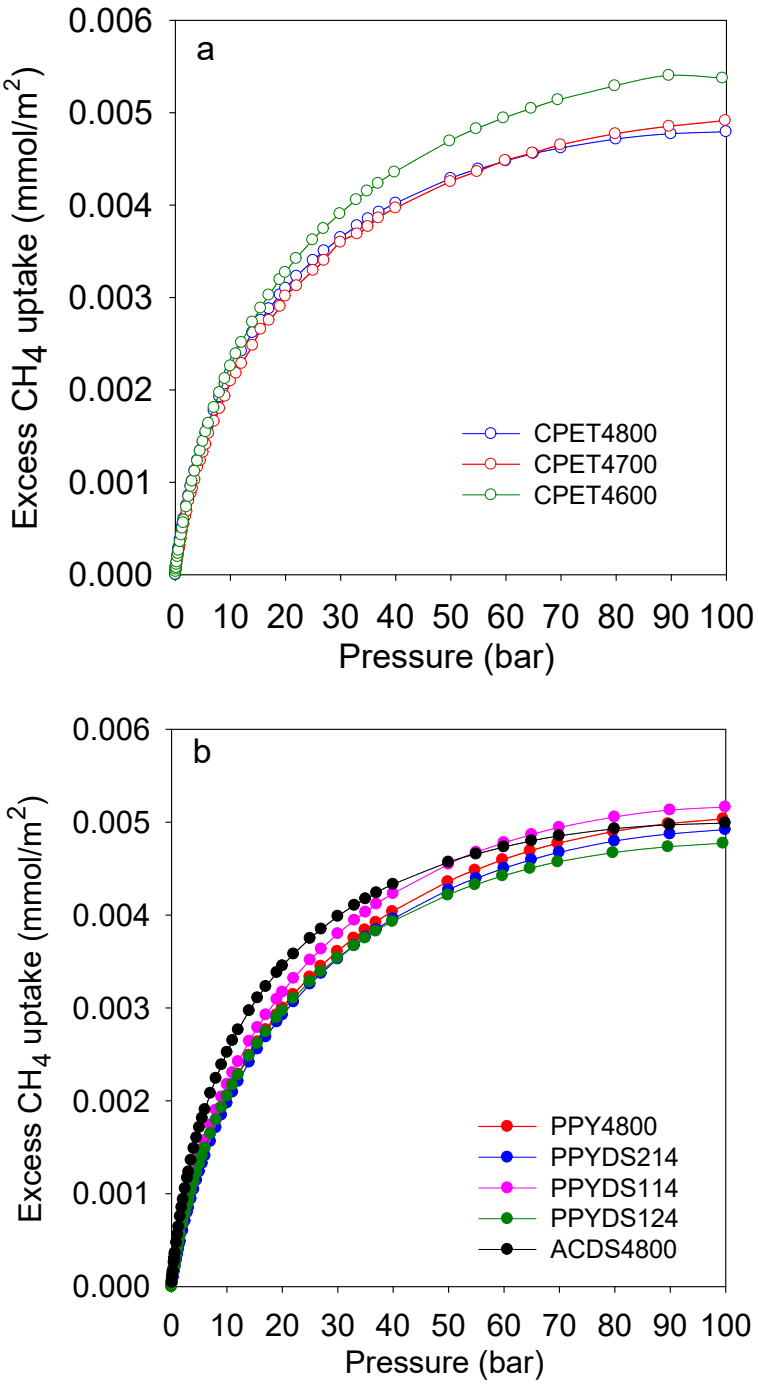

Supplementary Fig. 17 Methane uptake density of PET-derived CPET*4T* activated carbon composites, expressed as excess uptake per unit surface area. a, Methane uptake density of the PET-derived CPET*4T* activated carbon composites. b, The methane uptake density of a suite of fully carbonaceous activated carbons according to ref. 11. The methane uptake density of the carbon composites (a) is similar to that of the fully carbonaceous activated carbons (b).

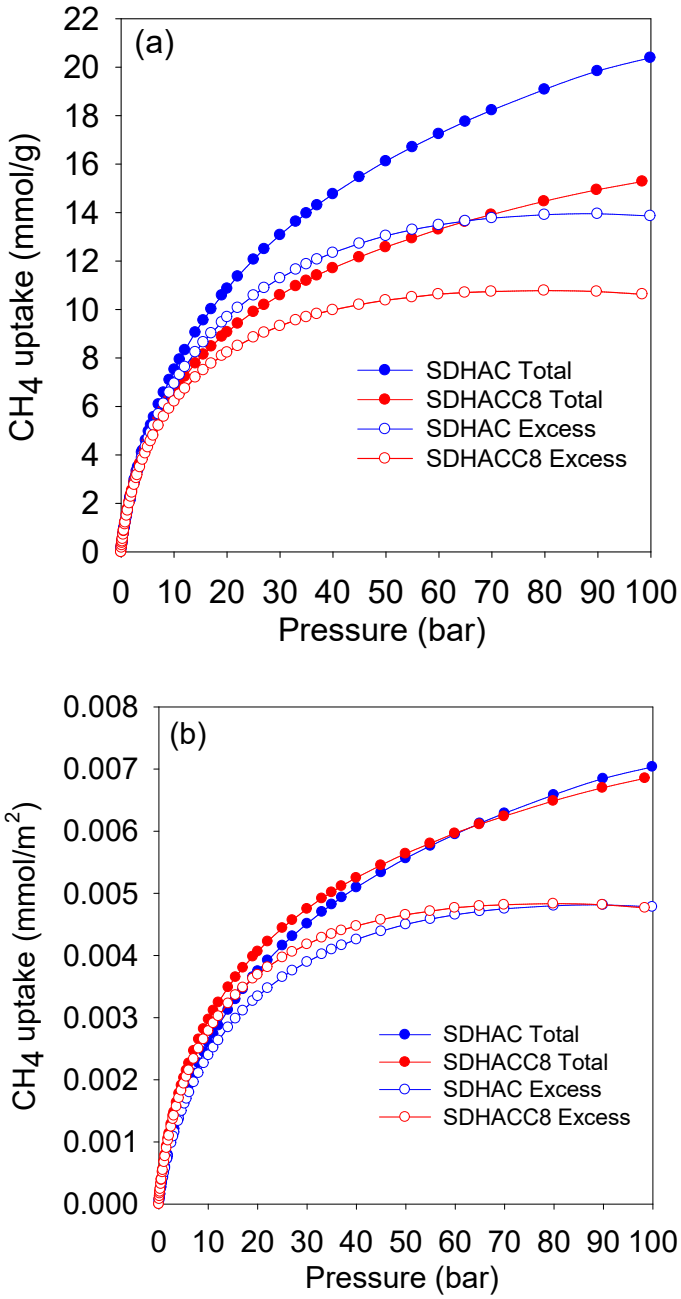

Supplementary Fig. 18 Gravimetric methane uptake (a) and gravimetric methane uptake density (b) of sawdust-derived activated carbon (SDHAC) and activated carbon composite (SDHACC8). The gravimetric uptake density, expressed as excess uptake per unit surface area, is similar for SDHAC and SDHACC8, and comparable to that of PET-derived CPET*4T* activated carbon composites and a suite of the fully carbonaceous activated carbons (Supplementary Fig. 17).

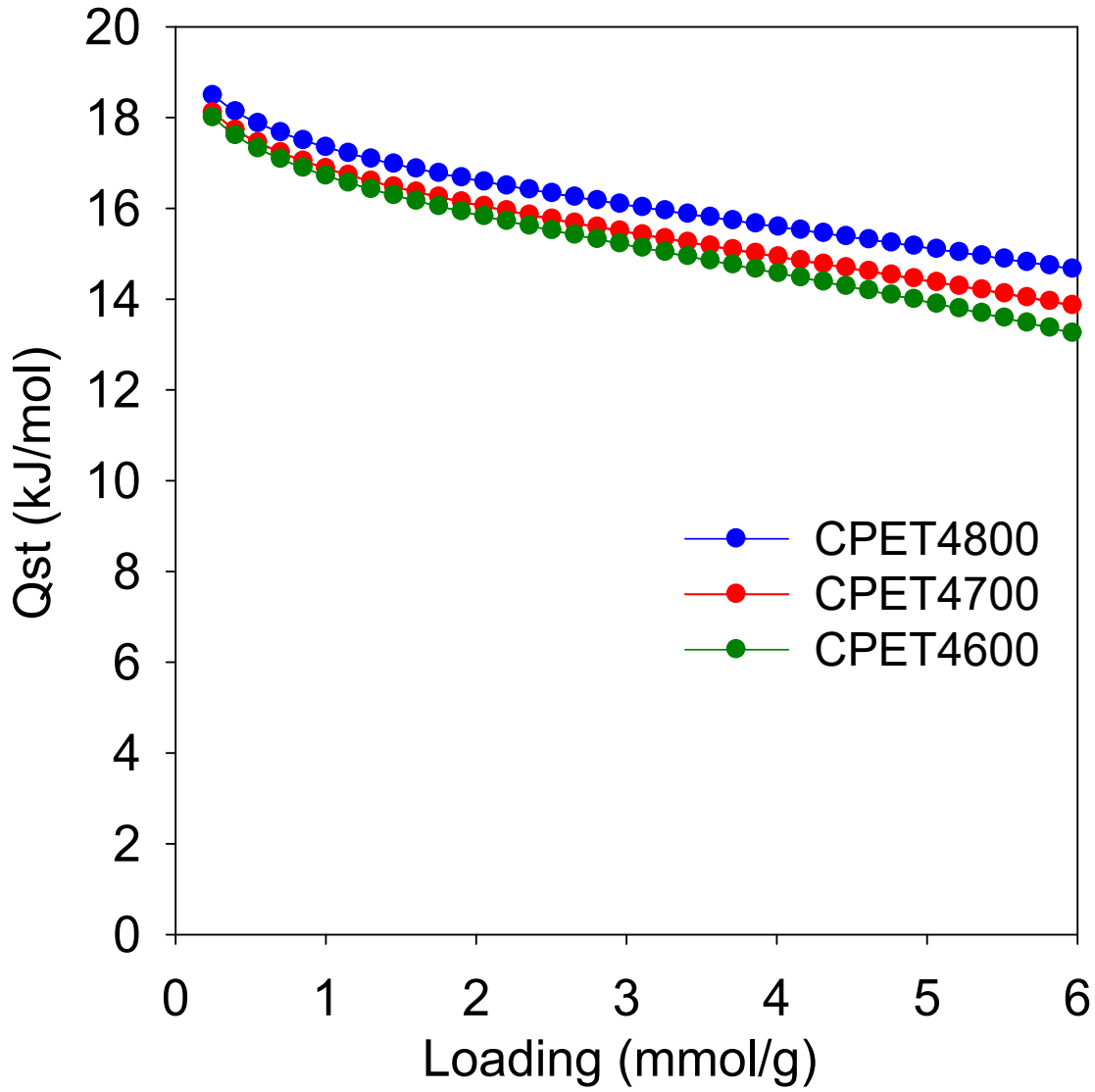

Supplementary Fig. 19 Isosteric heat of adsorption (Qst) as a function of methane loading of PET-derived activated carbon composites.

Supplementary References

1. A. Altwala and R. Mokaya, Predictable and targeted activation of biomass to carbons with high surface area density and enhanced methane storage capacity. *Energy Environ. Sci.*, 2020, **13**, 2967–2978.
2. A. Altwala and R. Mokaya, Modulating the porosity of activated carbons via pre-mixed precursors for simultaneously enhanced gravimetric and volumetric methane uptake. *J. Mater. Chem. A*, 2022, **10**, 13744–13757.
3. E. A. Hirst, A. Taylor and R. Mokaya, A simple flash carbonization route for conversion of biomass to porous carbons with high CO_2 storage capacity. *J. Mater. Chem. A*, 2018, **6**, 12393–12403.
4. E. Haffner-Staton, N. Balahmar and R. Mokaya, High yield and high packing density porous carbon for unprecedented CO_2 capture from the first attempt at activation of air-carbonized biomass. *J. Mater. Chem. A*, 2016, **4**, 13324–133335.
5. N. Balahmar, A. S. Al-Jumialy and R. Mokaya, Biomass to porous carbon in one step: directly activated biomass for high performance CO_2 storage. *J. Mater. Chem. A*, 2017, **5**, 12330–12339.
6. M. Sevilla, A. B. Fuertes and R. Mokaya, High density hydrogen storage in superactivated carbons from hydrothermally carbonized renewable organic materials. *Energy Environ. Sci*., 2011, **3**, 1400–1410.
7. W. Sangchoom and R. Mokaya, Valorization of lignin waste: Carbons from hydrothermal carbonization of renewable lignin as superior sorbents for CO_2 and hydrogen storage. *ACS Sustainable Chem. Eng.*, 2015, **3**, 1658–1667.
8. H. M. Coromina, D. A. Walsh and R. Mokaya, Biomass-derived activated carbon with simultaneously enhanced CO_2 uptake for both pre and post combustion capture applications. *J. Mater. Chem. A*, 2016, **4**, 280–289.
9. L. S. Blankenship, N. Balahmar and R. Mokaya, Oxygen-rich microporous carbons with exceptional hydrogen storage capacity. *Nat. Commun.*, 2017, **8**, 1545.
10. L. S. Blankenship and R. Mokaya, Cigarette butt-derived carbons have ultra-high surface area and unprecedented hydrogen storage capacity. *Energy Environ. Sci.*, 2017, **10**, 2552–2562.

11. N. Balahmar and R. Mokaya, Pre-mixed precursors for modulating the porosity of carbons for enhanced hydrogen storage: towards predicting the activation behaviour of carbonaceous matter. *J. Mater. Chem. A*, 2019, **7**, 17466– 17479.
12. J. A. Mason, M. Veenstra and J. R. Long, Evaluating metal–organic frameworks for natural gas storage. *Chem. Sci*., 2014, **5**, 32–51.
13. D. Alezi, Y. Belmabkhout, M. Suyetin, P. M. Bhatt, Ł. J. Weseliński, V. Solovyeva, K. Adil, I. Spanopoulos, P. N. Trikalitis, A.-H. Emwas and M. Eddaoudi, MOF crystal chemistry paving the way to gas storage needs: Aluminum-based soc-MOF for CH_4, O_2, and CO_2 storage. *J. Am. Chem. Soc*., 2015, **137**, 13308–13318.
14. H. Furukawa, N. Ko, Y. B. Go, N. Aratani, S. B. Choi, E. Choi, A. O. Yazaydin, R. Q. Snurr, M. O'Keeffe, J. Kim and O. M. Yaghi, Ultrahigh porosity in metal-organic frameworks. *Science*, 2010, **329**, 424-428.
15. Z. Chen, P. Li, R. Anderson, X. Wang, X. Zhang, L. Robison, L. R. Redfern, S. Moribe, T. Islamoglu, D. A. Gomez-Gualdron, T. Yildirim, J. F. Stoddart and O. K. Farha, Balancing volumetric and gravimetric uptake in highly porous materials for clean energy. *Science*, 2020, **368**, 297–303.
16. T. Tian, Z. Zeng, D. Vulpe, M. E. Casco, G. Divitini, P. A. Midgley, J. Silvestre-Albero, J. C. Tan, P. Z. Moghadam and D. Fairen-Jimenez, A sol-gel monolithic metal-organic framework with enhanced methane uptake. *Nat. Mater.*, 2018, **17**, 174–179.
17. B. M. Connolly, M. Aragones-Anglada, J. Gandara-Loe, N. A. Danaf, D. C. Lamb, J. P. Mehta, D. Vulpe, S. Wuttke, J. Silvestre-Albero, P. Z. Moghadam, A. E. H. Wheatley and D. Fairen-Jimenez, Tuning porosity in macroscopic monolithic metal-organic frameworks for exceptional natural gas storage, *Nat. Commun*., 2019, **10**, 2345.